Nanoscale

PAPER

Check for updates

Cite this: *Nanoscale*, 2020, **12**, 21440

In situ growth of CeO_2 on g-C_3N_4 nanosheets toward a spherical g-C_3N_4/CeO_2 nanozyme with enhanced peroxidase-like catalysis: a selective colorimetric analysis strategy for mercury(II)†

Xiaoting Zhao,‡ Shuai Li,‡ Xiaoxue Yu, Ruotong Gang and Hua Wang *

Received 16th July 2020,
Accepted 24th September 2020

DOI: 10.1039/d0nr05315e

rsc.li/nanoscale

Cerium dioxide (CeO_2) nanocatalysts were initially grown *in situ* on 2D graphitic carbon nitride (g-C_3N_4) nanosheets to yield the nanocomposites g-C_3N_4/CeO_2 with a spherical structure for the catalysis-based colorimetric analysis of Hg^{2+} ions in blood and wastewater. As the synergetic introduction of g-C_3N_4 nanosheets might promote the electron transfer in CeO_2, the resulting g-C_3N_4/CeO_2 nanozyme was found to present greatly enhanced catalytic activity, as demonstrated by the steady-state kinetic studies, which is nearly 4-fold higher than that of pure CeO_2. Moreover, the g-C_3N_4/CeO_2 nanozymes would aggregate in the presence of Hg^{2+} ions due to the strong interaction between Hg^{2+} and the nitrogen of g-C_3N_4, leading to a decrease of catalysis rationally depending on the Hg^{2+} ion concentration. A colorimetric analysis strategy is therefore developed for the selective detection of Hg^{2+} ions separately in the complex samples of blood and wastewater, showing a linear concentration range from 0.50 nM to 800 nM with the LOD of 0.23 nM as exemplified for Hg^{2+} ions in blood. Also, the recovery tests indicated that the developed colorimetric method can allow for the accurate analysis of Hg^{2+} ions in wastewater and blood. Such a route for the fabrication of composite nanozymes by growing catalytic nanomaterials on conductive 2D substrates may be extended to the design of other kinds of nanozymes with enhanced catalytic performances for developing catalysis-based detection platforms.

Introduction

Mercury as a widespread heavy metal in the environment can present high toxicity and severe adverse effects on human health.[1–3] Particularly, the water-soluble divalent mercuric ion (Hg^{2+}), the most usual and stable form of mercury, can accumulate in living organisms *via* the food chain causing serious damage to human kidneys, digestive system, and nervous systems.[4,5] Generally, the acceptable limit of Hg^{2+} ions in drinking water is about 1.0 μg L^{-1} set by the World Health Organization (WHO).[6] To date, numerous analytical strategies have been developed for the detection of Hg^{2+} ions by atomic spectroscopy,[7,8] optical sensing,[9,10] and electrochemical[11,12] and colorimetric analyses.[13,14] However, most of the current strategies encounter some problems like time-consuming operation, low sensitivity, and poor selectivity against the complicated background interference. Therefore, it is still of great interest to develop a rapid, sensitive, and selective analysis method for Hg^{2+} ions especially those in complex media like blood and wastewater.

Recent years have witnessed the wide applications of various nanozymes for the direct analysis of functional molecules and heavy metal ions through the efficient stimulation or specific inhibition of catalysis.[15–19] This kind of catalysis-based colorimetric methodology may possess some advantages in terms of simple operation, fast response, signal visibility, high sensitivity, and on-site analysis.[20,21] As an example, cerium oxide nanoparticles (CeO_2) with enzyme-like activity have been fabricated for developing various environmental pollutant detectors and biosensors.[22] For example, Zhang *et al.* have synthesized a kind of ceria nanozyme with the ability of significantly enhanced superoxide scavenging.[23] Qiu and co-authors have fabricated cerium oxide nanorod-templated metal–organic frameworks for the sensitive detection of Cr(VI).[24] Nevertheless, these nanozymes mostly still face the vital problem of low catalytic activity, which may greatly limit

Institute of Medicine and Materials Applied Technologies, College of Chemistry and Chemical Engineering, Qufu Normal University, Qufu, Shandong 273165, P. R. China. E-mail: huawang@qfnu.edu.cn

†Electronic supplementary information (ESI) available: SEM images of g-C_3N_4 nanosheets, XPS analysis, the catalytic kinetic results of g-C_3N_4/CeO_2, XRD analysis, recovery tests, the practical applications for detecting Hg^{2+} in wastewater samples and the comparison of analytical results among different documented methods. See DOI: 10.1039/d0nr05315e

‡These authors contributed equally to this work.

This journal is © The Royal Society of Chemistry 2020

their wide applications in the field of biochemical sensing. To solve the problems, considerable strategies have been proposed to improve the catalytic activity of nanozymes by regulating their sizes, morphologies, or compositions. For example, Qu *et al.* have studied the peroxidase-like activity of mesoporous CeO_2 nanorods, showing different catalytic performances depending on their morphologies.[25] Wei and co-authors also have reported an effective strategy for modulating the peroxidase-like activity of nanoceria by doping transition metals like manganese.[26] Moreover, graphitic carbon nitride (g-C_3N_4) nanosheets are cost-effective and conductive substrates with appealing features like excellent chemical and thermal stability, environmental friendliness, and a wonderful electronic structure.[27] As a result, g-C_3N_4 nanosheets have been widely used in the fields of photo-degradation of organic pollutants, photo-splitting of water, electrochemical sensors, and bio-imaging.[28,29] Yet, there are few reports on the use of g-C_3N_4 nanosheets for the regulation of nanozyme activities or as nanozyme catalysts. In particular, the free electron pairs of nitrogen on the surface of g-C_3N_4 nanosheets may act as active sites for the adsorption and analysis of heavy metal ions like Hg^{2+} ions.[13]

Inspired by the pioneering work above, herein, spherical nanocomposites of carbon nitride/cerium dioxide (g-C_3N_4/CeO_2) were synthesized by growing *in situ* CeO_2 on g-C_3N_4 nanosheets, with the procedure systemically illustrated in Scheme 1A. It was discovered that the resulting g-C_3N_4/CeO_2 nanocomposites could present greatly enhanced catalytic activity as compared with g-C_3N_4 or CeO_2, presumably because the synergetic introduction of g-C_3N_4 might increase the electron transfer in CeO_2. In the presence of Hg^{2+} ions, to our surprise, the catalytic activities of g-C_3N_4/CeO_2 will be largely inhibited, leading to the decrease of catalysis rationally depending on the Hg^{2+} ion concentration, with the main sensing procedure illustrated in Scheme 1B. A catalysis-based colorimetric strategy was thus developed for the selective detection of Hg^{2+} ions separately in blood and wastewater samples. To the best of our knowledge, this is the first report on the fabrication of nanocomposite nanozymes by the *in situ* growth of catalytic metal oxides like CeO_2 on conductive 2D substrates like g-C_3N_4 nanosheets towards nanocomposite nanozymes with enhanced catalysis for the design of different catalysis-based detection platforms for monitoring various biological species.

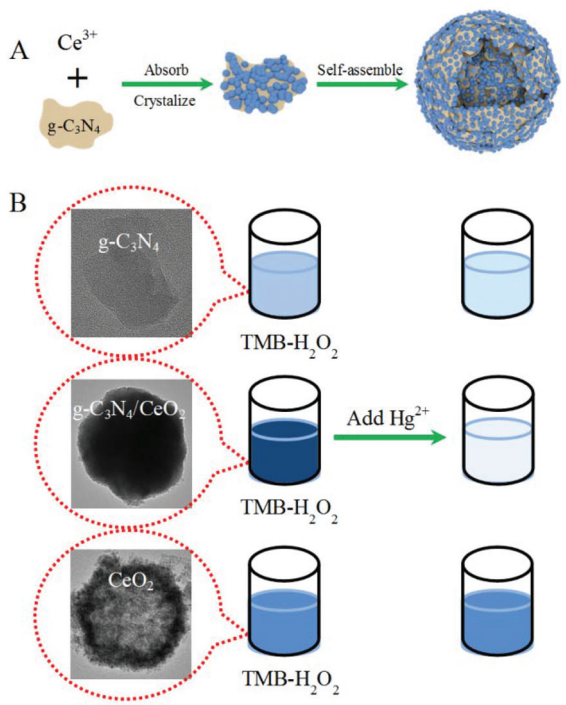

Scheme 1 Schematic illustration of (A) the preparation of g-C_3N_4/CeO_2 nanocomposites and (B) the colorimetric protocol of Hg^{2+} ions using g-C_3N_4/CeO_2 nanocomposites with Hg^{2+}-inhibited catalytic activity in catalyzing the TMB-H_2O_2 reactions, showing the changing colors of reaction solutions.

Experimental section

Reagents and chemicals

Melamine (MA), polyvinylpyrrolidone (PVP), cerium(III) nitrate hexahydrate $CeNO_3{\cdot}6H_2O$, ethylene glycol, 3,3′,5,5′-tetramethylbenzidine (TMB), L-cysteine (Cys), glutathione (GSH), L-lysine (Lys), L-histidine (His), L-tyrosine (Tyr), L-serine (Ser), threonine (Thr), valine (Val), arginine (Arg), leukocyte (Leu), dopamine (DA), ascorbic acid (AA) and uric acid (UA) were purchased from Sigma-Aldrich. Mercuric nitrate, lead nitrate, nickel nitrate, sodium acetate, citric acid, and hydrogen peroxide (H_2O_2, 30%) were purchased from Sinopharm Chemical Reagent Co. (China). All other chemicals were of analytical grade. Deionized water (18.2 MΩ cm, Millipore) was obtained from an ultrapure water system.

Apparatus

Scanning electron microscopy (SEM) images were collected on a Zeiss Sigma 500/VP microscope (Zeiss, Germany). Transmission electron microscopy (TEM) images were collected by using a Tecnai G20 microscope (FEI). Colorimetric measurements were performed with a microplate reader (Infinite M200 PRO, Tecan, Switzerland) with 96-well plates (JET BIOFIL, Guangzhou, China). UV-vis absorption spectra were recorded using a UV-3600 spectrophotometer (Shimadzu, Japan) equipped with a thermostated holder.

Preparation of bulk g-C_3N_4 and g-C_3N_4 nanosheets

Bulk g-C_3N_4 was prepared by the polymerization of melamine at high temperature. In detail, a certain amount of melamine was heated at 550 °C for 2 h under air with a ramp rate of about 2 °C min^{-1} for both the heating and cooling processes. Furthermore, the so-obtained yellow product bulk g-C_3N_4 was peeled to yield g-C_3N_4 nanosheets according to a modified procedure reported previously.[30]

Fabrication of g-C_3N_4/CeO_2 nanocomposites and CeO_2 nanospheres

g-C_3N_4/CeO_2 nanocomposites with a spherical structure were prepared by growing *in situ* CeO_2 on g-C_3N_4 nanosheets by the one-pot hydrothermal route. Typically, for g-C_3N_4/CeO_2 nanocomposites, an aliquot of g-C_3N_4 nanosheets, cerium nitrate hexahydrate (0.3333 g) and polyvinylpyrrolidone (0.1333 g) were dispersed in ethylene glycol solution (10 mL), and then deionized water (350 μL) was added under stirring. After being continuously stirred for 1 h, the clear solution was transferred to a 15 mL Teflon-lined autoclave to be heated at 160 °C for 8 h. Furthermore, the suspensions were cooled down to room temperature, and then collected by centrifugation at 12 000 rpm for 8 min, followed by washing with deionized water and ethanol sequentially. Finally, the yielded products were dried in a vacuum oven at 60 °C overnight as g-C_3N_4/CeO_2 nanocomposites. Besides, the synthesis of CeO_2 nanospheres was conducted by the same process, except that no g-C_3N_4 nanosheets were introduced in the first step.[31]

Catalytic activity measurements

The peroxidase-like catalytic activities of g-C_3N_4, CeO_2 and g-C_3N_4/CeO_2 nanozymes were comparatively studied by catalyzing the oxidation reactions of TMB in the presence of H_2O_2. Briefly, an aliquot of g-C_3N_4, CeO_2 or g-C_3N_4/CeO_2 (1.0 mg mL^{-1}, 10 μL) was added to acetate buffer (190 μL, 0.10 M, pH 4.0) containing 0.50 mM TMB and 1.0 M H_2O_2. Afterward, the absorbance values were monitored at 652 nm using a microplate reader. The experimental conditions of the catalytic reactions separately with g-C_3N_4, CeO_2 and g-C_3N_4/CeO_2 were optimized at different pH values, temperatures and reaction times.

Colorimetric analysis of Hg^{2+} ions

The colorimetric measurements were performed on g-C_3N_4/CeO_2 nanocomposites with and without Hg^{2+} ions. Generally, an aliquot of 5.0 μL of g-C_3N_4/CeO_2 nanocomposite (2.50 mg mL^{-1}) and Hg^{2+} ions (500 nM) was introduced into the TMB-H_2O_2 chromogenic system at room temperature for about 20 min. A 96-well plate and a microplate reader were used to record the UV-visible absorption value at 652 nm, and the blue reaction product was monitored. The responses of the g-C_3N_4/CeO_2 nanozyme-based analysis method to Hg^{2+} and other kinds of ions and molecules like Zn^{2+}, Cd^{2+}, Cu^{2+}, Pb^{2+}, Fe^{2+}, Co^{2+}, Ni^{2+}, Cr^{3+}, Ca^{2+}, and PO_4^{3-} (each 1.0 μM) were comparatively investigated.

Under the optimal conditions, the developed catalysis-based colorimetric method was used for the detection of Hg^{2+} with different concentrations in buffers. First, an aliquot of g-C_3N_4/CeO_2 nanozyme (2.50 mg mL^{-1}) was separately added to TMB-H_2O_2 solutions with different concentrations of Hg^{2+} ions. The reaction mixtures were incubated for 20 min, and the absorbance at 652 nm was recorded by using a micro-plate reader. Besides, different concentrations of Hg^{2+} ions spiked separately in blood and wastewater samples were analyzed with the same procedure.

Results and discussion

Preparation and characterization of different nanomaterials

The g-C_3N_4/CeO_2 nanocomposites were fabricated simply by growing *in situ* CeO_2 on g-C_3N_4 nanosheets by the one-pot hydrothermal route, with the possible procedure systemically illustrated in Scheme 1A. As can be seen from Scheme 1A, Ce^{3+} ions first adsorbed on the surface of the g-C_3N_4 nanosheets to form precursor nanoparticles, and then under the action of surfactants spherical nanocomposites of g-C_3N_4/CeO_2 were formed. The morphology and microstructure of the so-prepared g-C_3N_4/CeO_2 nanocomposites were comparably characterized by scanning electron microscopy (SEM) and transmission electron microscopy (TEM) imaging (Fig. 1). It is clearly noted that CeO_2 nanomaterials could display uniformly defined monodisperse hollow nanospheres with a size of about 200 nm in diameter (Fig. 1A), as confirmed by the TEM image displayed in the amplified view (Fig. 1B). More interestingly, when CeO_2 was grown on the g-C_3N_4 nanosheets, which may intrinsically possess an irregular layered structure (Fig. S1A†), the yielded g-C_3N_4/CeO_2 nanocomposites could illustrate the spherical morphology with a diameter of about 360 nm (Fig. 1C–E). Furthermore, Fig. 1E reveals the morphological structure of g-C_3N_4/CeO_2 nanocomposites in the presence of Hg^{2+} ions. To our surprise, the spherical g-C_3N_4/CeO_2 nanocomposites might be collapsed to yield large aggregated

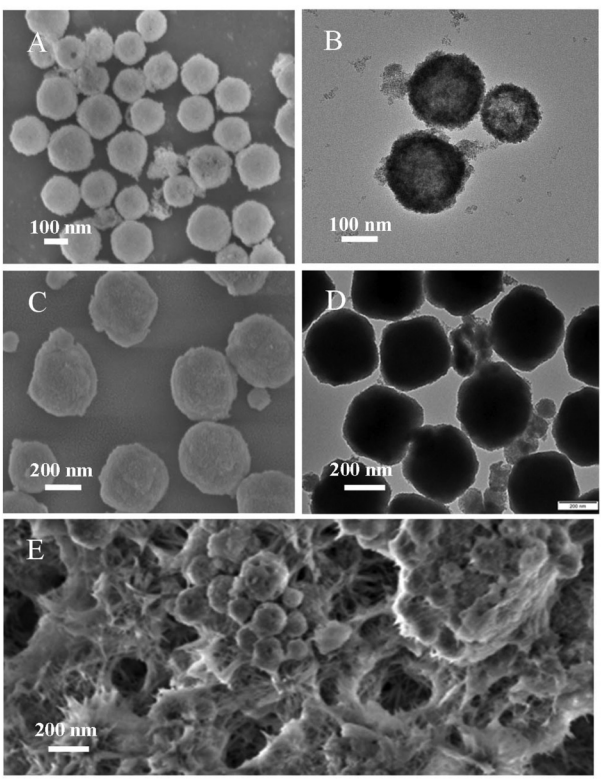

Fig. 1 SEM images and TEM images of CeO_2 (A and B) and g-C_3N_4/CeO_2 nanocomposites (C and D), and (E) SEM image of g-C_3N_4/CeO_2 after adding Hg^{2+} ions.

This journal is © The Royal Society of Chemistry 2020

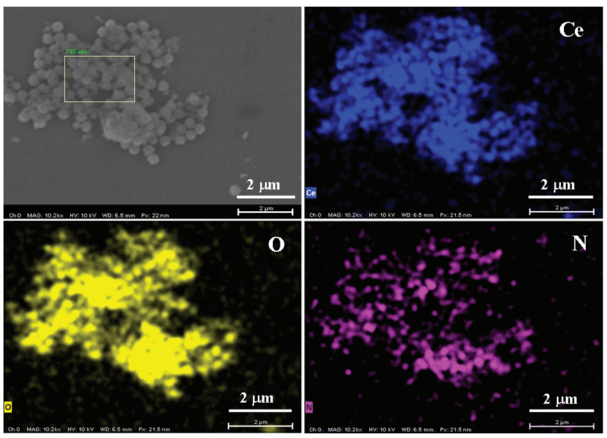

Fig. 2 The mapping analysis of different elements (Ce, O and N) for g-C_3N_4/CeO_2.

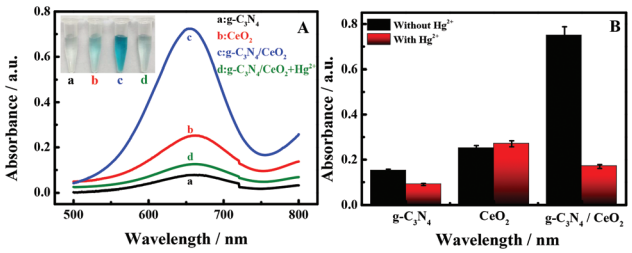

Fig. 3 Comparison of (A) UV-visible spectra of catalytic reaction products among (a) g-C_3N_4, (b) CeO_2, g-C_3N_4/CeO_2 (c) before and (d) after adding Hg^{2+} ions (inset: the photographs of the corresponding product solutions of catalytic TMB reactions); (B) comparison of the catalytic performances among g-C_3N_4, CeO_2 and g-C_3N_4/CeO_2 in catalyzing TMB-H_2O_2 reactions.

blocks, which might be ascribed to the strong covalent bonds between Hg^{2+} and the N in g-C_3N_4/CeO_2 nanocomposites. Moreover, elemental mapping analysis was performed for the obtained g-C_3N_4/CeO_2 nanocomposites (Fig. 2). One can see that elements Ce, O and N could be homogeneously distributed throughout the g-C_3N_4/CeO_2 framework, indicating the successful synthesis of the g-C_3N_4/CeO_2 nanocomposites. Besides, the analysis of the crystallographic structure of the prepared g-C_3N_4 nanosheets and g-C_3N_4/CeO_2 was performed by X-ray diffraction (XRD), with the results shown in Fig. S1B.† It was noted from Fig. S1B† (curve a) that g-C_3N_4 nanosheets could present a (002) peak only, demonstrating that layered g-C_3N_4 nanosheets should be successfully exfoliated. After the *in situ* growth of CeO_2 on g-C_3N_4 nanosheets, the diffraction peaks at 33.1°, 47.5° and 56.3° appeared, which can be assigned to the (200), (220), and (311) planes of CeO_2, respectively, indicating the formation of g-C_3N_4/CeO_2 nanocomposites (Fig. S1B curve b†).[32] Besides, the BET surface area of the developed g-C_3N_4/CeO_2 was found to be 34.23 $m^2\ g^{-1}$.

To gain further insight into the composition and chemical states of the Ce element in g-C_3N_4/CeO_2, XPS analysis was performed, with the data shown in Fig. S2.† Accordingly, the survey spectrum in Fig. S2A confirmed the presence of the C, N, O, and Ce elements in g-C_3N_4/CeO_2 nanozymes, as can be seen more clearly from Fig. S2B–E.† Also, five pairs of spin–orbit coupling of the Ce 3d spectra should be assigned to two orbits $3d_{3/2}$ and $3d_{5/2}$, labeled as u and v, respectively (Fig. S2E†). Among them, v, v_2, v_3, u, u_2, and u_3 might be attributed to Ce^{4+}, while v_0, v_1, u_0, and u_1 might have resulted from Ce^{3+}.[33] These data demonstrate that Ce^{4+} and Ce^{3+} might also coexist in the developed g-C_3N_4/CeO_2 nanozymes.

Comparative investigation of the peroxidase-like catalysis of g-C_3N_4/CeO_2 nanocomposites

The peroxidase-like catalytic properties of g-C_3N_4, CeO_2 and g-C_3N_4/CeO_2 were comparably investigated by catalyzing TMB-H_2O_2 chromogenic reactions (Fig. 3A). One can see that g-C_3N_4 nanosheets can display a little catalytic activity for the oxidation of TMB in the presence of H_2O_2 (curve a). Meanwhile, CeO_2 shows a relatively high catalytic activity compared to g-C_3N_4, but it is still relatively low (curve b). Moreover, the peroxidase-like catalytic activity of the resulting g-C_3N_4/CeO_2 nanozymes is greatly enhanced, which is nearly 4-fold higher than that of pure CeO_2 (curve c), as revealed by the reaction solution with a deeper blue color (Fig. 3A, inset), presumably because the synergetic introduction of g-C_3N_4 might increase the electron transfer in CeO_2. When Hg^{2+} ions were introduced into the g-C_3N_4/CeO_2 reaction solutions, the interaction between Hg^{2+} and the N of g-C_3N_4 might trigger the aggregation of g-C_3N_4/CeO_2 with a collapsed structure, thereby causing a decrease in the catalysis of g-C_3N_4/CeO_2 nanozymes in the catalytic TMB-H_2O_2 reactions (curve d).[34] The main sensing procedure for sensing Hg^{2+} ions is illustrated in Scheme 1B.

Furthermore, in order to verify the proposed detection mechanism of the developed catalysis-based strategy, the catalytic activities of g-C_3N_4, CeO_2 and g-C_3N_4/CeO_2 in the absence and presence of Hg^{2+} ions were comparably investigated by catalyzing the TMB oxidation in the presence of H_2O_2 (Fig. 3B). One can see that the catalytic activity of g-C_3N_4 nanosheets might decrease to a certain extent in the presence of Hg^{2+} ions, which is consistent with the phenomenon of g-C_3N_4/CeO_2 catalysis. However, the catalytic activity of CeO_2 might still remain basically unchanged in the presence of Hg^{2+} ions. Therefore, the above data indicate that it is the g-C_3N_4 in g-C_3N_4/CeO_2 nanocomposites, instead of CeO_2, that might have interacted with Hg^{2+} ions to cause a decrease in the catalytic activity of g-C_3N_4/CeO_2 nanocomposites.

To understand the enhanced peroxidase-like activity of g-C_3N_4/CeO_2, the steady-state kinetics was investigated in comparison with that of CeO_2 (Fig. S3 and S4†). Within the suitable range of H_2O_2 and TMB concentrations, the typical Michaelis–Menten curves of CeO_2 (Fig. S3A and C†) and g-C_3N_4/CeO_2 (Fig. S4A and C†) were thereby obtained. Furthermore, the apparent Michaelis–Menten parameters were calculated using the typical Lineweaver–Burk double reciprocal curves (Fig. S3B, D and S4B, D†). The so-obtained values of the

Michaelis constant (K_m) and maximal reaction velocity (V_m) are summarized in Table S1.† It is found that the K_m values of g-C_3N_4/CeO_2 are lower than that of CeO_2, showing a higher affinity for both H_2O_2 and TMB. Moreover, the V_m values of g-C_3N_4/CeO_2 are much higher than those of CeO_2, confirming that the introduction of g-C_3N_4 greatly improves the peroxidase-like catalytic activity of CeO_2. In addition, comparative investigations indicate that g-C_3N_4/CeO_2 could possess even higher substrate affinity than HRP.

To further understand the catalytic mechanism of the developed g-C_3N_4/CeO_2 nanozymes, the effects of reactive oxygen species typically like $^{\bullet}OH$ and $^{\bullet}O_2^-$ have been investigated by using the $^{\bullet}OH$ probe of p-phthalic acid (TA) and the $^{\bullet}O_2^-$ probe of hydroethidine (HE), respectively (Fig. S5†). It can be seen from Fig. S5A† that the addition of various amounts of g-C_3N_4/CeO_2 to H_2O_2 might cause no enhancement in the fluorescence intensities of the hydroethidine products, suggesting that $^{\bullet}O_2^-$ might not be produced from H_2O_2 in the g-C_3N_4/CeO_2-catalyzed reactions. However, the fluorescence intensity of TA-induced reaction products could apparently increase with increasing the g-C_3N_4/CeO_2 concentrations, indicating that $^{\bullet}OH$ could be effectively generated from H_2O_2 in the g-C_3N_4/CeO_2-catalyzed reactions (Fig. S5B†).

Optimization of the main colorimetric analysis conditions for Hg^{2+} assays

The main colorimetric analysis conditions of g-C_3N_4/CeO_2 nanozymes for Hg^{2+} ion detection were investigated from the absorbance changes of the products of catalytic reactions in comparison with those of g-C_3N_4 and CeO_2, including pH values, temperature, reaction time and concentration of the g-C_3N_4/CeO_2 nanozyme (Fig. 4). The pH value-dependent catalysis of g-C_3N_4/CeO_2 was comparatively investigated, revealing that for g-C_3N_4/CeO_2, g-C_3N_4 and CeO_2 showed more effective catalysis at lower pH values, ideally at pH 4.0 (Fig. 4A). Furthermore, the temperature-dependent catalysis of g-C_3N_4/CeO_2 in the Hg^{2+} ion detection was studied by taking g-C_3N_4 and CeO_2 as comparison (Fig. 4B). Accordingly, the developed g-C_3N_4/CeO_2 nanozymes exhibited the highest catalytic performance at a temperature of about 37 °C. Besides, as shown in Fig. 4C, the optimal time for the catalytic reactions was found to be about 20 min. Finally, as shown in Fig. 4D, the colorimetric response to Hg^{2+} ions might increase as the dosages of g-C_3N_4/CeO_2 nanozyme increased till 2.50 mg mL^{-1}. Therefore, 2.50 mg mL^{-1} of g-C_3N_4/CeO_2 nanozymes should be considered to be the optimal concentration in the experiment.

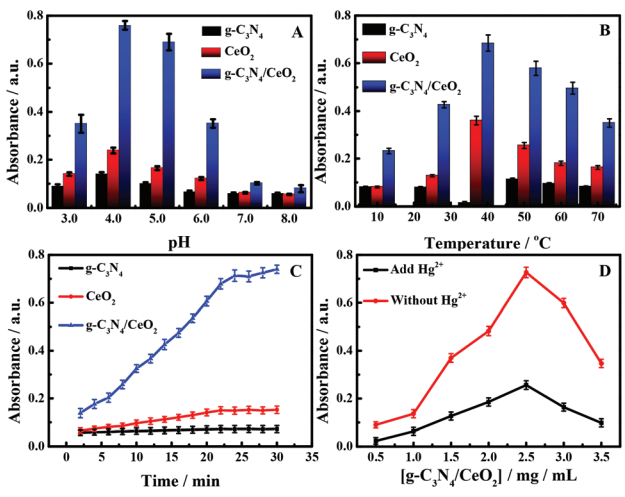

Fig. 4 Optimization of the main colorimetric analytical conditions for sensing Hg^{2+}, including (A) pH, (B) reaction temperature, (C) reaction time, and (D) g-C_3N_4/CeO_2 amounts, where the UV absorbance values of g-C_3N_4/CeO_2 were recorded at a wavelength of 652 nm.

Detection performances of the g-C_3N_4/CeO_2 nanozyme-based colorimetric assays for Hg^{2+} ions

Considering the possible interference of other kinds of substances in complex media like blood and wastewater, the responses of the g-C_3N_4/CeO_2 nanozyme-based analytical strategy to Hg^{2+} ions and other kinds of small molecules and ions were comparatively investigated, with the results shown in Fig. 5. One can see that the responses to other possibly coexisting substances might be negligibly low as compared with that of Hg^{2+} ions. Therefore, the developed g-C_3N_4/CeO_2 nanozyme-based colorimetric strategy can promise the highly selective detection of Hg^{2+} ions, especially those in complex samples like blood and wastewater. The high selectivity of the g-C_3N_4/CeO_2 nanozyme for Hg^{2+} ions is thought to result from the fact that Hg^{2+} ions may have much interaction with the nitrogen of g-C_3N_4 of the nanozyme, as evidenced by that of Hg^{2+} with amino groups. It is established that Hg^{2+} can have higher stability constants (K_f) with amino groups ($\log K_f$ = 19.3) than transition metal ions, such as Zn^{2+}, Co^{2+}, Ni^{2+} and Cd^{2+}, whose $\log K_f$ values are 8.70, 4.39, 8.01 and 6.65, respectively.[35] As a result, Hg^{2+} might selectively induce much larger aggregation of g-C_3N_4/CeO_2 by forming the N-Hg^{2+}-N structure towards the decreased catalysis of the g-C_3N_4/CeO_2 nanozyme. Yet, the detailed mechanism should be further investigated in the future.

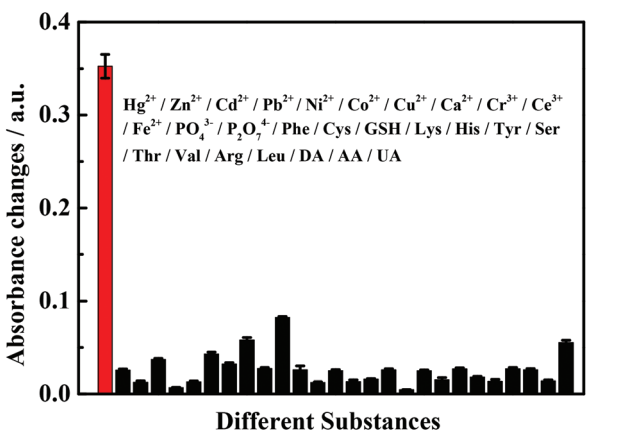

Fig. 5 g-C_3N_4/CeO_2 catalysis-based colorimetric responses to different ions (1.0 μM) and small molecules (1.0 μM) indicated.

This journal is © The Royal Society of Chemistry 2020

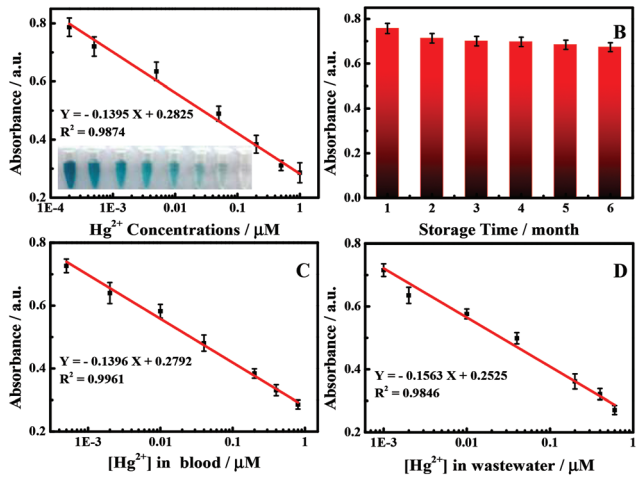

Fig. 6 Calibration curves of the relationships between the absorbance responses and different concentrations of Hg^{2+} ions in (A) buffer, (C) spiked blood and (D) spiked wastewater samples. (B) The storage stability of g-C_3N_4/CeO_2 for the Hg^{2+} analysis separately stored in the dark for different time intervals.

Under the optimal conditions, the developed g-C_3N_4/CeO_2 nanozyme-based colorimetric strategy was used for the detection of Hg^{2+} ions in acetate buffer (Fig. 6). It was found that with the increase of Hg^{2+} concentrations in buffer, the absorbance values of the catalytic reaction products gradually decreased, as more apparently displayed in the photographs of the corresponding solutions (Fig. 6, inset). A linear relationship was thus obtained for the determination of Hg^{2+} ions, showing the linear concentrations ranging from 0.20 nM to 1.0 μM, with the limit of detection (LOD) of about 0.085 nM, as estimated by the 3σ rule. In addition, the storage stability of the g-C_3N_4/CeO_2 nanozyme was also investigated (Fig. 6B). Unsurprisingly, no significant change in the absorbance value of the catalytic reaction solution was observed, even when the g-C_3N_4/CeO_2 nanozyme was stored for up to 6 months, proving the long-term stability of the nanozymes.

Colorimetric analysis of Hg^{2+} ions in samples

The catalysis-based colorimetric strategy was used for the analysis of Hg^{2+} ions with various concentrations separately spiked in human blood and industrial wastewater samples (Fig. 6C and D). Fig. 6C shows the absorbance value of the catalytic reaction solution responses *versus* Hg^{2+} ion concentrations in blood ranging from 0.50 nM to 800 nM, with the LOD of 0.23 nM. Moreover, Hg^{2+} ions in wastewater were also analyzed, showing the linear concentrations ranging from 1.0 nM to 600 nM, with the LOD of 0.42 nM. Moreover, the recovery tests were performed by using the developed colorimetric method to probe Hg^{2+} ions spiked in wastewater and blood samples. It was found that the detected Hg^{2+} ion concentrations could be considerably close to those of the added Hg^{2+} ions, showing the favourable recoveries obtained ranging from about 94.6–96.8% in wastewater samples (Table S2†) and 96.9–106.4% in blood samples (Table S3†). Therefore, the developed g-C_3N_4/CeO_2 nanozyme-based colorimetric method can allow for the selective detection of Hg^{2+} ions in complex samples like blood and wastewater. In addition, the analytical performances of the catalysis-based colorimetric method are compared with those of other analytical methods reported previously, with the results summarized in Table S4.†[13,36–38] One can note that the developed g-C_3N_4/CeO_2 nanozyme-based method exhibits better or comparable analytical performance in terms of detection ranges and LODs. Therefore, the developed g-C_3N_4/CeO_2 nanozyme-based colorimetric method can allow for the efficient evaluation of Hg^{2+} ions in complex samples like blood and wastewater.

Conclusions

In summary, spherical g-C_3N_4/CeO_2 nanocomposites were successfully synthesized by growing *in situ* CeO_2 on g-C_3N_4 nanosheets. A catalysis-based colorimetric method was further developed for analyzing Hg^{2+} ions separately in blood and wastewater by using g-C_3N_4/CeO_2 nanozymes. It was found that the synergetic introduction of g-C_3N_4 nanosheets might promote electron transfer in CeO_2 so as to endow the resulting g-C_3N_4/CeO_2 nanozymes with greatly improved catalytic activity, as compared with g-C_3N_4 or CeO_2. Also, g-C_3N_4 nanosheets were initially used as the recognition unit for Hg^{2+} ions in the colorimetric analytical strategy with g-C_3N_4/CeO_2 nanozymes. Moreover, the prepared spherical g-C_3N_4/CeO_2 nanozymes were demonstrated to present higher stability than most of the current catalytic nanocomposites commonly fabricated by the physically mixing route, so as to expect better reproducibility of the colorimetric detection of Hg^{2+} ions. The so-developed colorimetric strategy can facilitate the direct detection of Hg^{2+} ions separately in blood and wastewater, with the levels down to 0.23 nM and 0.42 nM, respectively. What's more, the detection performance of the developed method is comparatively better than those of most of the other colorimetric methods documented. Yet, the detailed mechanism for the Hg^{2+}-inhibited catalysis of g-C_3N_4/CeO_2 nanozymes should be further explored in the future. Importantly, such a fabrication route for spherical catalytic nanocomposites by growing CeO_2 nanocatalysts on the 2D carriers of g-C_3N_4 nanosheets may be extended to the design of other kinds of nanozymes with enhanced catalytical performance for developing catalysis-based detection platforms in various fields of clinical evaluation, environmental detection, food safety monitoring, and catalysis-based analytical applications.

Conflicts of interest

There are no conflicts to declare.

Acknowledgements

This work is supported by the National Natural Science Foundations of China (No. 22074079 and 21675099), the Major

Basic Research Program of the Natural Science Foundation of Shandong Province (No. ZR2018ZC0129), P. R. China, and the Special Fund for Post-doctoral Innovation Projects of Shandong Province (No. 201903045), P. R. China.

Notes and references

1 T. Li, S. Dong and E. Wang, *Anal. Chem.*, 2009, **81**, 2144–2149.
2 C. Guo and J. Irudayaraj, *Anal. Chem.*, 2011, **83**, 2883–2889.
3 S. Zhang, D. Zhang, X. Zhang, D. Shang, Z. Xue, D. Shan and X. Lu, *Anal. Chem.*, 2017, **89**, 3538–3544.
4 J. Yang, Y. Zhang, L. Zhang, H. Wang, J. Nie, Z. Qin, J. Li and W. Xiao, *Chem. Commun.*, 2017, **53**, 7477–7480.
5 Z. Sun, N. Zhang, Y. Si, S. Li, J. Wen, X. Zhu and H. Wang, *Chem. Commun.*, 2014, **50**, 9196–9199.
6 J. Han, R. Fu, C. Jin, Z. Li, M. Wang, P. Yu and Y. Xie, *Microchem. J.*, 2020, **152**, 104356.
7 L. Wu, Z. Long, L. Liu, Q. Zhou, Y. I. Lee and C. Zheng, *Talanta*, 2012, **94**, 146–151.
8 A. Thongsaw, Y. Udnan, G. M. Ross and W. C. Chaiyasith, *Talanta*, 2019, **197**, 310–318.
9 Z. Liu, W. Jin, F. Wang, T. Li, J. Nie, W. Xiao and Y. Zhang, *Sens. Actuators, B*, 2019, **296**, 126698.
10 Y. Zhang, S. Guo, Z. Jiang, G. Mao, X. Ji and Z. He, *Anal. Chem.*, 2018, **90**, 9796–9804.
11 C. Lai, S. Liu, C. Zhang, G. Zeng, D. Huang, L. Qin, X. Liu, H. Yi, R. Wang, F. Huang, B. Li and T. Hu, *ACS Sens.*, 2018, **3**, 2566–2573.
12 S. L. Jiokeng, L. M. Dongmo, E. Ymélé, D. B. Nde and I. K. Tonlé, *Electrochim. Acta*, 2019, **316**, 152–161.
13 H. Liu, S. Li, L. Feng, Y. Hua, Y. Cai, M. Yin, Y. Wan and H. Wang, *J. Hazard. Mater.*, 2020, **388**, 121798.
14 C. Song, J. Li, Y. Sun, X. Jiang, J. Zhang, C. Dong and L. Wang, *Sens. Actuators, B*, 2020, **310**, 127849.
15 S. Li, X. Zhao, X. Yu, Y. Wan, M. Yin, W. Zhang, B. Cao and H. Wang, *Anal. Chem.*, 2019, **91**, 14737–14742.
16 S. Li, X. Zhao, R. Gang, B. Cao and H. Wang, *Anal. Chem.*, 2020, **92**, 5152–5157.
17 H. Qiu, F. Pu, X. Ran, C. Liu, J. Ren and X. Qu, *Anal. Chem.*, 2018, **90**, 11775–11779.
18 J. Wu, X. Wang, Q. Wang, Z. Lou, S. Li, Y. Zhu, L. Qin and H. Wei, *Chem. Soc. Rev.*, 2019, **48**, 1004–1079.
19 X. Wang, X. Gao, L. Qin, C. Wang, L. Song, Y. Zhou, G. Zhu, W. Cao, S. Lin, L. Zhou, K. Wang, H. Zhang, Z. Jin, P. Wang, X. Gao and H. Wei, *Nat. Commun.*, 2019, **10**, 704.
20 S. Li, L. Zhang, Y. Jiang, S. Zhu, X. Lv, Z. Duan and H. Wang, *Nanoscale*, 2017, **9**, 16005–16011.
21 H. Wang, S. Li, Y. Si, Z. Sun, S. Li and Y. Lin, *J. Mater. Chem. B*, 2014, **2**, 4442–4448.
22 H. Cheng, S. Lin, F. Muhammad, Y.-W. Lin and H. Wei, *ACS Sens.*, 2016, **1**, 1336–1343.
23 Y. Li, X. He, J. J. Yin, Y. Ma, P. Zhang, J. Li, Y. Ding, J. Zhang, Y. Zhao, Z. Chai and Z. Zhang, *Angew. Chem., Int. Ed.*, 2015, **54**, 1832–1835.
24 Y. Wang, R. P. Liang and J. D. Qiu, *Anal. Chem.*, 2020, **92**, 2339–2346.
25 Z. Tian, J. Li, Z. Zhang, W. Gao, X. Zhou and Y. Qu, *Biomaterials*, 2015, **59**, 116–124.
26 W. Guo, M. Zhang, Z. Lou, M. Zhou, P. Wang and H. Wei, *ChemCatChem*, 2019, **11**, 737–743.
27 X. Zhang, X. Xie, H. Wang, J. Zhang, B. Pan and Y. Xie, *J. Am. Chem. Soc.*, 2013, **135**, 18–21.
28 M. Li, L. Zhang, X. Fan, M. Wu, M. Wang, R. Cheng, L. Zhang, H. Yao and J. Shi, *Appl. Catal., B*, 2017, **201**, 629–635.
29 H. Kim, D. Lim, N. H. Kwon, S. Son, S. Choi, J. Kim, S. J. Hwang and S. Park, *ACS Appl. Energy Mater.*, 2020, **3**, 4812–4820.
30 M. Vazquez-Gonzalez, W. C. Liao, R. Cazelles, S. Wang, X. Yu, V. Gutkin and I. Willner, *ACS Nano*, 2017, **11**, 3247–3253.
31 Y. Long, S. Song, J. Li, L. Wu, Q. Wang, Y. Liu, R. Jin and H. Zhang, *ACS Catal.*, 2018, **8**, 8506–8512.
32 X. She, H. Xu, H. Wang, J. Xia, Y. Song, J. Yan, Y. Xu, Q. Zhang, D. Du and H. Li, *Dalton Trans.*, 2015, **44**, 7021–7031.
33 C. Korsvik, S. Patil, S. Seal and W. Self, *Chem. Commun.*, 2007, **10**, 1056–1058.
34 J. Ge, J. Xiao, L. Liu, L. Qiu and X. Jiang, *J. Porous Mater.*, 2016, **23**, 791–800.
35 Y. Ma, L. Jiang, Y. Mei, R. Song, D. Tian and H. Huang, *Analyst*, 2013, **138**, 5338.
36 W. R. Cui, C. R. Zhang, W. Jiang, R. P. Liang, S. H. Wen, D. Peng and J. D. Qiu, *ACS Sustainable Chem. Eng.*, 2019, **7**, 9408–9415.
37 J. S. Lee, M. S. Han and C. A. Mirkin, *Angew. Chem., Int. Ed.*, 2007, **46**, 4093–4096.
38 J. Zhu, B. Z. Zhao, Y. Qi, J. J. Li, X. Li and J. W. Zhao, *Sens. Actuators, B*, 2018, **255**, 2927–2935.

 This journal is © The Royal Society of Chemistry 2020